IASI observations of sulfur dioxide (SO$_2$) in the boundary layer of Norilsk

Sophie Bauduin[1], Lieven Clarisse[1], Cathy Clerbaux[1,2], Daniel Hurtmans[1] and

Pierre-François Coheur[1]

[1]Spectroscopie de l'atmosphère, Service

de Chimie Quantique et Photophysique,

Université Libre de Bruxelles, Brussels,

Belgium

[2]UMPC Univ. Paris 6; Université

Versailles St-Quentin; CNRS/INSU;

LATMOS-IPSL, Paris, France

Abstract.   Norilsk is one of the most polluted cities in the world, largely because of intense mining of heavy metals. Here we present satellite observations of SO_2 in a large area surrounding the city, derived from four years of measurements from the Infrared Atmospheric Sounding Interferometer (IASI), the nadir thermal infrared (TIR) sounder onboard the MetOp platforms. TIR instruments are conventionally considered to be inadequate for monitoring near-surface composition, because their sensitivity to the lowest part of the atmosphere is limited by the thermal contrast between the ground and the air above it. We demonstrate that IASI is capable of measuring SO_2 (here as a partial column from 0 to 2 km) in Norilsk, thanks to the large temperature inversions and the low humidity in wintertime. We discuss the influence of thermal contrast and of surface humidity on the SO_2 retrieved columns, and estimate the retrieval errors. Using a simple box model, we derive the yearly total emissions of SO_2 from Norilsk and compare them to previously reported values. More generally, we present in this work the first large scale demonstration of the capability of space-based TIR sounders to measure near-surface SO_2 anthropogenic pollution.

1. Introduction

Measuring the composition of the planetary boundary layer (PBL) is essential for monitoring pollutants and, using the synergy with models, for quantifying anthropogenic emissions and understanding their impacts on our environment and climate (e.g. [*Laj et al.*, 2009]). Satellite remote sensing is especially appealing for monitoring boundary layer pollution, as it allows to acquire spatial distributions of different trace species simultaneously and enables to evaluate their temporal variations [*Martin*, 2008]. Sensing the PBL is however challenging as the concentrations of these gases are generally weak and confined to a small part of the atmospheric column. For TIR sounders, the sensitivity to the PBL depends in addition on the temperature difference between the surface and the air above (the so-called thermal contrast). When this difference is small, TIR sounders inherently have a low sensitivity to the surface concentration [*Deeter et al.*, 2007]. On the other hand, it has been demonstrated that TIR sounders can have a good sensitivity to the surface when there is a large thermal contrast [*Deeter et al.*, 2007; *Clarisse et al.*, 2010].

Despite this, there have been only limited efforts to exploit the measurements of TIR sounders to specifically probe the polluted boundary layer. Even less attention has been given to satellite observations performed in situations where temperature inversions occur in the boundary layer, although those thermal contrast conditions are favorable as well. This was illustrated in particular with the retrieval of ammonia (NH_3), a short-lived species usually confined in the lowest layers [*Clarisse et al.*, 2010]. The first global nighttime measurements of NH_3 support and extend these findings [*Van Damme et al.*, 2013].

In a recent work, *Boynard et al.* [2014] have demonstrated the capability of IASI to detect several pollutants simultaneously during an extreme winter smog event in China. In this work, we explore such situations more thoroughly, and we particularly exploit large negative thermal contrasts associated with strong temperature inversions, occurring in the Arctic. We focus on the industrial area of Norilsk, situated in northwestern Siberia. This region is well-known for the extraction of heavy metals (Nickel, Copper, ...) and for its extreme levels of pollution, which are directly responsible for the degradation and contamination of the surrounding environment [*Vlasova et al.*, 1991; *Blais et al.*, 1999; *Tutubalina and Rees*, 2001; *Allen-Gil et al.*, 2003; *Zubareva et al.*, 2003] and which contribute to the Arctic air pollution [*Law and Stohl*, 2007; *Hirdman et al.*, 2010]. Indeed, Norilsk's smelters emit each year significant quantities of heavy metals in the atmosphere [*Boyd et al.*, 2009; *Fukasawa et al.*, 2000] but also of acidifying gases, especially sulfur dioxide (SO$_2$) [*AMAP*, 1998; *Fukasawa et al.*, 2000; *AMAP*, 2006]. UV sounders, which are well known to be able to probe the boundary layer [*Carn et al.*, 2004, 2007; *Krotkov et al.*, 2008; *Li et al.*, 2010; *Lee et al.*, 2011; *Fioletov et al.*, 2011; *McLinden et al.*, 2012], have previously measured enhancements of SO$_2$ in this area [*Khokhar et al.*, 2004, 2005; *Walter et al.*, 2012]. Here, we report measurements of Norilsk's SO$_2$ pollution by IASI. This is the first large scale observation of near-surface SO$_2$ by a nadir infrared hyperspectral sounder.

In the next section, we briefly present the IASI instrument and investigate its sensitivity to anthropogenic SO$_2$. In section 3, the method used to retrieve SO$_2$ concentrations in the Norilsk region is presented. The discussion of the results is given in section 4. Spatial distributions, time series and winter emissions of SO$_2$ are discussed in the three first

subsections and errors are separately discussed in the last subsection. Finally in section 5, conclusions are drawn.

2. IASI instrument and sensitivity to surface SO$_2$

IASI is a Michelson interferometer on board the MetOp-A platform, launched in 2006 in a sun-synchronous polar orbit. A successor on MetOp-B was launched on 17th September 2012 and a third one is foreseen on MetOp-C in 2017. MetOp has local equator crossing times of 09:30 and 21:30, and a swath of 2200 km, allowing global coverage twice a day. The IASI effective field of view is composed of 2x2 footprints, each of 12 km diameter at nadir. IASI measures the upwelling radiance emitted by the Earth and the atmosphere in the spectral range 645–2760 cm^{-1} with a resolution of 0.5 cm^{-1} after apodization. More details about the instrument are given elsewhere [*Clerbaux et al.*, 2009; *Hilton et al.*, 2012]. The primary goal of IASI is helping numerical weather prediction by providing temperature and water vapor profiles with high precision and vertical resolution [*Schlüssel et al.*, 2005; *August et al.*, 2012]. Furthermore, IASI was also designed to provide data on the atmospheric composition and has already proven its extraordinary capability to monitor trace gases, with more than 20 species observed [*Clarisse et al.*, 2011a]. Among them, SO$_2$ has three vibrational bands in the spectral domain covered by the instrument, namely the intense ν_3 band centered at 1362 cm^{-1}, the ν_1 band centered at 1152 cm^{-1} and the weaker $\nu_1 + \nu_3$ band at 2500 cm^{-1}. In the TIR, SO$_2$ has principally been detected in tropospheric volcanic plumes, characterized by large SO$_2$ concentrations at altitudes where the sounders have their maximum sensitivity [*Clarisse et al.*, 2008; *Karagulian et al.*, 2010; *Haywood et al.*, 2010; *Clarisse et al.*, 2012].

Until recently, SO$_2$ from anthropogenic emissions has only been detected by TIR instruments in the troposphere, following uplift of boundary layer pollution [*Clarisse et al.*, 2011b]. The first report of SO$_2$ at near-surface level from IASI has been made by *Boynard et al.* [2014] using the methodology developed for the present study. Low sensitivity of IASI to near-surface SO$_2$ pollution is due for a large part to the general unfavorable small thermal contrasts encountered, but also to the opacity of the atmosphere due to water in the spectral region of the strong ν_3 band. As a consequence, two conditions need to be simultaneously fulfilled to detect SO$_2$ from TIR observations: a sufficiently high thermal contrast and low humidity. Both are found in the Norilsk region, as illustrated in Figure 1b for an example scene, and in Figure 3 (two bottom panels) for a 4-years time series: in the lowest layers the water mixing ratio in winter is indeed generally well below 0.2 g/kg, while the thermal inversion can be as high as -15 K. To demonstrate the effect of these conditions on the measurements, two spectra have been compared in Figure 1a (for the scene characterized by temperature and humidity as shown in Figure 1b). The IASI spectrum is shown in blue and a corresponding simulated spectrum, for which we assumed an atmosphere free of SO$_2$, is represented in red. The difference between these two spectra (green curve in Figure 1a) shows spectral features in emission between 1320 and 1390 cm^{-1} well above the noise (of about 4×10^{-7} W/(m^2 sr m^{-1}) in this spectral range, *Clerbaux et al.* [2009]; *Hilton et al.* [2012]), which are characteristic of SO$_2$ (see orange curve in Figure 1a) situated in a part of the atmosphere where the air temperature is larger than that of the surface. The fact that SO$_2$ is observed in emission is consistent with the presence of thermal inversions. Note in addition that the temperature inversion prevents vertical transport and therefore traps air pollutants close to the surface. As a

107 final remark, we have also analyzed the sensitivity of IASI to boundary layer SO$_2$ using the

108 spectral signatures of SO$_2$ in its ν_1 band, which is much less influenced by water vapour.

109 However, the ν_1 band is weaker than the ν_3 band by a factor of 7.8 if the intensities of

110 the strongest lines are compared (from HITRAN database 2008, [*Rothman et al.*, 2009]).

111 This weakness of the ν_1 band is such that it is detected only for very high levels of SO$_2$

112 and very large thermal contrasts. We focus therefore hereafter on the ν_3 band region only.

3. Retrieval method

3.1. Method

113 The method for retrieving near-surface SO$_2$ concentrations in Norilsk from IASI mea-

114 surements is largely based on the one presented in *Carboni et al.* [2012]. It relies on

115 the optimal estimation framework [*Rodgers*, 2000], which traditionally consists of simul-

116 taneous iterative adjustment of the atmospheric parameters of interest and spectrally

117 interfering unknown variables. However, the latter can also be interpreted as part of the

118 spectral noise and accounted for in a generalized noise covariance matrix. While complete

119 information on these interfering unknowns is not available, often there is some a priori

120 information. To exploit this, a generalized covariance matrix can be constructed from

121 the difference between observed spectra and forward simulated spectra (see *Carboni et al.*

122 [2012] for details). In this way, a mean difference **c** and associated covariance matrix $\mathbf{S}_\epsilon$

123 can be calculated, representative for our missing information on the interfering unknowns

124 (these include the IASI noise, forward model errors, errors in the meteorological fields and

125 errors coming from the lack of knowledge of the parameters affecting radiance spectra).

The cost function J that is minimized during the retrieval then takes the form

$$J \;=\; (\mathbf{y} - \mathbf{F}(\mathbf{x}, \mathbf{b}) - \mathbf{c})^{\mathrm{T}} \mathbf{S}_{\epsilon}^{-1}(\mathbf{y} \;-\; \mathbf{F}(\mathbf{x}, \mathbf{b}) \;-\; \mathbf{c}) \;+\; (\mathbf{x} - \mathbf{x_a})^{\mathrm{T}} \mathbf{S_a}^{-1}(\mathbf{x} \;-\; \mathbf{x_a}) \quad (1)$$

where $\mathbf{x}$ is the reduced state vector (see section 3.3), $\mathbf{x_a}$ is the a priori state vector and $\mathbf{S_a}$ is the associated a priori covariance matrix, $\mathbf{b}$ is the vector containing all the fixed parameters affecting the measurement $\mathbf{y}$, $\mathbf{F}$ is the forward model.

3.2. Spectral error covariance matrix $\mathbf{S}_{\epsilon}$

Three $\mathbf{S}_{\epsilon}$ matrices have been built to represent three different periods for the Norilsk region, according to values of thermal contrasts and humidity (Figure 3, bottom panels). These periods correspond to the winter (here taken from November to March), characterized by high negative thermal contrasts and low water vapor content in the boundary layer, the summer (June to August) with low positive thermal contrasts and the highest humidities, and the mid-season (April-May, September-October) representing intermediate thermal contrasts and humidity values. Note that it would have been possible to use only one $\mathbf{S}_{\epsilon}$ for these three periods but it would have included large variability, which would have caused higher errors on SO$_2$ retrieved columns [*Carboni et al.*, 2012].

To calculate the $\mathbf{S}_{\epsilon}$ for each period, about 20000 IASI spectra from 2010 and 2011 have been used. Only those with less than 25% of cloud coverage (information taken from EUMETSAT L2 products, [*August et al.*, 2012]) and with no detectable SO$_2$ were selected. For this, observed spectra relatively far from the source region were used (60–62°N/75–100°E and 74–75°N/75–100°E). This area usually does not exhibit observable quantities of SO$_2$ (see Figure 2). In addition, to account for possible residual transported SO$_2$ plumes from volcanic origin, data was filtered using a brightness temperature difference (BTD) sensitive to SO$_2$ [*Clarisse et al.*, 2008]. The corresponding simulated spectra were calculated for the spectral range 1330–1390 cm^{-1} with the Atmosphit software [*Coheur*

$_{147}$ *et al.*, 2005]. Temperature and humidity profiles used in the simulations were taken from

$_{148}$ EUMETSAT L2 products [*Schlüssel et al.*, 2005; *August et al.*, 2012]. This was also the

$_{149}$ case for the surface temperature, if available. When surface temperature was not included

$_{150}$ in the L2, it was evaluated by averaging the BT of six window channels (857.50, 866.25,

$_{151}$ 868.50, 879.00, 892.75, 1231.75 cm^{-1}). Vertical profiles of other atmospheric constituents

$_{152}$ have been taken from the standard subarctic models (winter and summer) [*Anderson*

$_{153}$ *et al.*, 1986] defining average volume mixing ratios (vmr) for CH$_4$ and nitrous oxide (N$_2$O),

$_{154}$ that mainly absorbe the radiation in the covered spectral range along with water. The

$_{155}$ CH$_4$ model profile was scaled by a factor of 1.06, to bring surface vmr to 1800 ppm, in

$_{156}$ agreement with surface measurements (see e.g. http://www.esrl.noaa.gov/gmd/aggi/).

3.3. Retrieval parameters

$_{157}$ Just as for forward simulations, retrievals have been performed with the Atmosphit

$_{158}$ software in the spectral range 1330–1390 cm^{-1} and on spectra with less than 25% of cloud

$_{159}$ coverage. The chosen reduced state vector **x** contains two SO$_2$ columns, the first one

$_{160}$ extending from 0 to 2 km and the second one from 2 to 5 km. We expect indeed negligible

$_{161}$ amounts of SO$_2$ above 5 km, given the short lifetime of this gas in general. Furthermore,

$_{162}$ more specifically for the winter cases analyzed here, the presence of strong temperature

$_{163}$ inversions confines the pollution at near-surface level. The standard subarctic SO$_2$ profile

$_{164}$ [*Anderson et al.*, 1986] has been used for the a priori profile but a large variability of

$_{165}$ 150% has been considered for the diagonal elements of the a priori covariance matrix **S$_a$**,

$_{166}$ to allow retrievals of high concentrations which occur frequently [*AMAP*, 2006]. The off-

$_{167}$ diagonal elements have been calculated using an exponential decay with 7 km correlation

$_{168}$ length. The **fixed** parameters have been chosen the same as for the forward simulations.

169 The complete retrieval scheme has been applied on IASI spectra recorded for four years,

170 between the 1st January 2008 and the 31st December 2011 in a large area around Norilsk

171 (61–75°N/75–96°E and 67–75°N/96–100°E).

4. Results and discussion

4.1. Spatial distribution

172 Figure 2 presents the spatial distribution of the average retrieved 0–2 km column of SO$_2$

173 for February 2009. The highest mean retrieved columns are above 2 Dobson Units (1 DU=

174 2.69×10^{16} molecules/cm^2) and situated above the city. The plume spreads away from the

175 source, as seen by a gradual decrease of the retrieved concentrations. Averaged over one

176 month, it seems that the pollution plume follows two distinctive transport pathways, one

177 eastward and the other westward, surrounding the mountains. The entire SO$_2$ plume

178 observed by IASI covers a large region of about 165 000 km^2 around Norilsk, suggesting a

179 significant influence on its surrounding environment, as discussed in *Vlasova et al.* [1991];

180 *Tutubalina and Rees* [2001] and *Zubareva et al.* [2003]. It is worth noting that we can

181 distinctly observe the plume following the Plutorana Plateau (the concentrations above

182 300 m never being higher than 0.5 DU). This clearly demonstrates that the detected

183 SO$_2$ is located close to the surface, where the temperature inversions develop. Actually,

184 the mean altitude of these inversion layers, calculated over the whole retrieved area for

185 February 2009, and based on the temperature profiles provided by EUMETSAT L2, is

186 410 m above the ground. Most of the SO$_2$ pollution is thus probably being transported

187 below this altitude. Similar SO$_2$ distributions can be drawn for other winter months.

188 However, during summer and mid-season, higher humidity and lower thermal contrasts

189 hamper measurement of near-surface SO$_2$. The detection is only possible for some days,

190 with particular favorable conditions (see also Figure 3). In contrast, during the winter

191 and as shown in Figure 3 (discussed next), thermal contrasts and humidity are quite

192 homogenously favorable in the area. We can thus reasonably assume that, during winter

193 months, our mean retrieved SO$_2$ columns are representative of near-surface SO$_2$ amounts.

4.2. Time series

194 Time series of the surface retrieved SO$_2$ column are presented in Figure 3 (first panel)

195 for the period 01/01/2008–31/12/2011. For each day, the 0–2 km column is an average

196 of all columns in a circle of 50 km radius centered on Norilsk. However, in summer

197 and mid-season notably, average columns can be strongly underestimated due to changes

198 in PBL sensitivity, and thus do not correspond to the real pollution above the area.

199 Moreover, the average is made over a quite large area around Norilsk and is thus not

200 very representative of the high concentrations of SO$_2$ just above the city. Therefore,

201 daily maximum SO$_2$ columns are also presented in Figure 3 (second panel). The two

202 last panels show the mean thermal contrasts, calculated as the difference between the

203 temperature of the surface and of the air at 350 m altitude (both temperature are from

204 the operational L2) above the ground, and mean humidity (at 350 m), calculated over

205 the same area as the SO$_2$ columns and for the same period. The altitude of 350 m above

206 the ground was chosen to be equal to the average altitude of the temperature inversion

207 (calculated here for the area of interest and only for winter months), below which most

208 of the gas is probably located and which is also the altitude where the peak sensitivity

209 is expected. In Figure 3, the SO$_2$ measurements from morning and evening overpasses

210 have been averaged together. In wintertime, solar radiation at the latitude of Norilsk is

211 low (or even vanishing during the Polar Night) and surface, atmospheric temperatures,

and humidity are similar during day and night (see green and red curves in the two last

panels of Figure 3). Therefore, the IASI sensitivity to boundary layer SO$_2$ is identical in

the two cases. However, in summer, the diurnal variability of temperatures and humidity

is high: differences of more than 10 K of thermal contrast and of more than 5 g/kg of

water vapor occur from one day to the next (Figure 3). This variability is such that the

sensitivity can be very different between the two IASI overpasses, leading to differences

in SO$_2$ measurements. For the same reasons as those explained above, calculating an

average concentration for the mid-season and summer periods, which are already difficult

to retrieve due to the weaker sensitivity, produces large underestimation. This is well seen

in Figure 3, with the average concentrations from May to October being below 5 DU and

essentially close to 0, while daily maximum values can be significantly larger, typically up

to 10 DU and in few cases even 50 DU. It can be seen from Figure 3 that retrievals during

the summer and the mid-season have been possible for days (morning and/or evening)

combining exceptionnally low humidity and high thermal contrasts (in absolute value).

Both conditions coexist for example in April 2008, August 2008, September 2008, July

2009, April 2010, May 2010, July 2010 and May 2011. Note that in August 2008, most

of the detected SO$_2$ was probably emitted by the Kasatochi eruption and transported

over the Norilsk's region [*Karagulian et al.*, 2010]. Mid-season and summer retrieved SO$_2$

columns are hence only qualitatively discussed in the following.

Although the number of successful retrievals is much larger in winter owing to the

more favorable conditions for detecting boundary layer pollution, we observe also a large

variability of SO$_2$ columns. Daily means range from 0.04 DU (the a priori column) to about

20 DU in February 2011. Most columns however vary between 1 and 5 DU. Maximum

columns reach 50 DU on several days. It clearly appears that most days for which SO$_2$ concentrations are close to the a priori correspond to situations where IASI measurements are not sensitive to the boundary layer, when thermal contrasts are close to zero. Humidity stays low for the entire winter and therefore does not contribute to the loss of sensitivity. This kind of unfavorable winter episodes occur for instance in January 2008, end of March 2008, November 2008, January 2009, beginning of November 2009, November 2010, end of January 2011, end of March 2011, December 2011.

There are several previous reports of SO$_2$ measurements in Norilsk, which were made either by surface instruments [*Fukasawa et al.*, 2000], airplanes [*Walter et al.*, 2012] or satellites, but in the latter cases using reflected solar radiation in the UV-Vis [*Walter et al.*, 2012; *Fioletov et al.*, 2013]. Table 1 summarises the different available SO$_2$ measurements and compares them to this work. Although the direct comparison is difficult because they are not colocated in time and space and refer to different quantities (surface concentrations or vmr, integrated columns), we find that our values are in good agreement with these, especially with the vertical columns reported by *Walter et al.* [2012], which were retrieved from UV satellite measurements. Our retrieved SO$_2$ concentrations are in contrast smaller than those measured by *Fukasawa et al.* [2000] and those reported by the *AMAP* [2006] during the 90's. This is likely due to the fact that these concentrations were measured at the surface while our averaged concentrations were calculated over a 0–2 km layer. As we have demonstrated above, the main SO$_2$ column is likely to be confined to a smaller layer, and therefore our reported SO$_2$ concentrations are biased low. This difference could also be explained by potential reductions of Norilsk's SO$_2$ emissions. For instance, *Walter et al.* [2012] referring to a report of the Norwegian Council on Ethics [*Council on Ethics*

for the Government Pension Fund Global, 2009], mention that the company MMC Norilsk Nickel, which is the head of Norilsk smelting facilities, planned to reduce its SO$_2$ emissions by 70% by 2010, even though the same report states that '[...] no significant decrease in SO$_2$ emissions have so far been observed'. Although the comparison provided here may be evidence of the impact of emission regulations, a definitive conclusion would require more investigation and validation of the IASI measurements.

4.3. Winter emissions

From the IASI SO$_2$ measurements, we have estimated the winter emissions of the Norilsk sources. We have first calculated daily SO$_2$ total masses M according to the relation:

$$M(SO_2) = \frac{M_{SO_2} C_{SO_2} S}{N_a} \qquad (2)$$

where M_{SO_2} is the molar mass of SO$_2$ (64.0638 g/mol), C_{SO_2} is the mean SO$_2$ total column (here calculated as the sum of the 0-2 km and 2-5 km retrieved columns) in molecules/cm^2 for the chosen box of surface area S, and N_a is the Avogadro number. SO$_2$ masses have been calculated for each 0.25°×0.25° box of a grid covering the entire retrieved area (60–75°N/75–100°E), and then summed to obtain the SO$_2$ total mass for the region. To avoid underestimation of the total masses because of lack of sensitivity on some days in winter (obvious in Figure 3 from the low column averages), only measurements with thermal contrast higher or equal than 10 K in absolute value were taken into account. Averaged SO$_2$ columns were then interpolated from one month of data, for each box of the grid. In this way, a mean daily total mass for the entire region is estimated for each month.

The emissions for the winter months have then been calculated using a simple box model and first order loss terms [*Jacob*, 1999]:

$$E_{i+1}(SO_2) = \frac{M_{i+1}(SO_2) - M_i(SO_2)e^{-t/\tau_{\text{eff}}}}{\tau_{\text{eff}}(1 - e^{-t/\tau_{\text{eff}}})} \tag{3}$$

E_i and $M_i(SO_2)$ are respectively the emission and total mass of SO_2 for the day i, τ_{eff} is the effective lifetime of SO_2, and t is time between two observations (here one day). Because we have estimated a mean daily total mass for each month, the previous equation simplifies in $E = M/\tau_{\text{eff}}$ and leads to constant daily emissions for each month. The calculation has only been done for winter months (November to March), for which the IASI sensitivity to boundary layer is the highest. Only emissions calculated for 2009 are discussed hereafter, because this year presents the largest and the most constant amount of available data.

The choice of the lifetime is crucial in estimating the emission. *Lee et al.* [2011] have calculated the seasonal zonal mean lifetime of SO_2 in the boundary layer using the GEOS-Chem model. They show that it is very variable with season and latitude, mainly because of changes in dry deposition velocities and in supply of oxidants. For high latitudes, a lifetime of about one day in summer to more than 3 days in winter was obtained. In wintertime and particularly during the Polar night, SO_2 lifetime is longer than for the summer, because of smaller concentrations of oxidants and reduced velocities of dry deposition due to snow coverage [*Chin and Jacob*, 1996; *Wesely*, 2007]. Here, we used a SO_2 lifetime of three days representative of winter conditions.

Table 2 compares SO_2 emissions derived in this work and in other studies. Emissions for 2009 from IASI add up to 0.46 Mt in the winter and 1.10 Mt for the whole year. Yearly totals were calculated from the winter months, assuming constant emissions. This is a

reasonable assumption as smelting facilities usually run continuously (24 hours per day, 7 days per week). This value is in good agreement with *Khokhar et al.* [2008] and *Walter et al.* [2012]. Total emissions reported in *Blacksmith Institutes* [2007] and *Fioletov et al.* [2013] are about a factor two larger. However the latter study uses a rather short SO$_2$ lifetime of five hours. It is also possible that the winter SO$_2$ lifetime is larger than the three days which we have used. It is clear that SO$_2$ lifetime has to be better constrained to make more accurate estimation of emissions from satellite measurements.

4.4. Estimation of the retrieval error

In this section, we estimate the error on the IASI retrieved SO$_2$ columns independently of the diagnostics of the Optimal Estimation method, which are highly dependent on the a priori constraints. As there are also no suitable independent measurements available for validation, an alternative approach has been developed based on retrievals of a set of synthetic IASI spectra with known SO$_2$ columns. This allows a rigorous estimate of the errors characterized by the global error spectral covariance matrix $\mathbf{S}_\epsilon$, which includes the IASI noise, uncertainties in relevant meteorological parameters, in the spectroscopy of interfering trace gases and radiative transfer.

The synthetic IASI spectra have been generated with 340 randomly chosen SO$_2$ columns and representative surface temperatures, temperature and humidity profiles for the winter months in Norilsk. Then a synthetic noise was added, generated from the multivariate normal distribution corresponding to the $\mathbf{S}_\epsilon$ matrix. From these spectra, SO$_2$ was retrieved in exactly the same way as for the observed IASI spectra. The relative difference between the input and the retrieved columns then gives the error term described above. A histogram of the errors as a function of thermal contrast (in absolute value) and the

0–2 km SO$_2$ column is shown in Figure 4. A clear dependence of the errors on the thermal contrast is observed: for thermal contrasts above 12 K the errors range from 10% to 40%, between 20% to 85% for thermal contrasts between 6 and 12 K and finally above 80% for thermal contrasts below 6 K. When thermal contrast is small there is little sensitivity to PBL SO$_2$ and the retrieval depends only on the choice of the a priori. As it increases, sensitivity to the PBL increases and the retrieved values match closer the real ones. The magnitude of the SO$_2$ columns also has an effect on the sensitivity, as larger columns yield larger spectral signatures and hence larger signal to noise ratio's. This can be seen in Figure 4, where the distinction was made for columns below (blue columns) and above (orange columns) 5 DU. However, even for very large thermal contrasts and large columns, there is a low bias of about 15% for the larger SO$_2$ columns. This difference could be due to an imperfect training set used in the generation of the $\mathbf{S}_\epsilon$ matrix (e.g. with residual SO$_2$ signatures present). Another possibility is that the presence of spectral interferences, irrecoverably masks part of the SO$_2$ signature, and hence leads to an underestimation of the SO$_2$ column. Overall, relative errors are on average below 30% for thermal contrasts exceeding 12 K, a result which shows that thermal infrared sounders can in favourable conditions probe the PBL with high accuracy. We also investigated the influence of water vapour on the retrieval as larger H$_2$O columns are expected to adversely affect the retrieval. However, wintertime conditions in Norilsk are dry (less than 1 g/kg of H$_2$O at 350 m) and constant, so that no dependence was found here.

One category of errors not accounted for here, relates to the strength of the SO$_2$ spectral signature (for a given column). These include errors in the spectroscopic parameters, uncertainties on the SO$_2$ profile and the impact of the thermal contrast on the SO$_2$ lines

in the forward model. Independent validation would be required to properly estimate

such errors.

5. Conclusions

We have obtained the first IASI distributions of SO$_2$ at near-surface level, using 4-year of

measurements in a large area (61–75°N/75–96°E and 67–75°N/96–100°E) around the pol-

luted city of Norilsk in the Arctic circle. Retrievals were performed using a methodology

based on the Optimal Estimation and where a full $\mathbf{S}_\epsilon$ spectral variance-covariance matrix

was used to account for interfering atmospheric parameters. Time series of the retrieved

SO$_2$ 0–2 km partial column have been investigated and revealed a strong dependence of

the sensitivity of IASI to the polluted surface layer on thermal contrast and humidity.

In wintertime, when there is a combination of dry conditions and frequent temperature

inversions, large SO$_2$ columns (around 5 DU on average but up to 50 DU occasionally)

have been successfully retrieved for many days. In favorable conditions retrieval errors

can be as low as 10%, but depending on thermal contrast and SO$_2$ column, can reach

up to 95%. In the summer months, retrievals are harder due to lower values of thermal

contrast coupled with larger atmospheric humidity, which renders the atmosphere opaque

in the lowest layers. For some days in summer, however, successful retrievals have been

obtained, giving daily maximum SO$_2$ columns typically between 5 and 20 DU. It is worth

emphasizing that measurements provided in winter by TIR sounders such as IASI largely

complement observations of UV instruments at high latitudes regions, as the sounding of

the latter is impossible during this period as solar radiation is unavailable.

The yearly emissions of SO$_2$ for the Norilsk area have been estimated from the retrieved

columns in the winter months, using a simple box model and first order loss terms, and

assuming constant emissions. For a lifetime of three days, we obtained a yearly emission of 1.10 Mt. This value is in reasonable agreement with those obtained by other satellite sounders operating in the UV-visible and other type of remote-sensing instruments. Validation of the SO$_2$ measurements of this work and a better evaluation of the lifetime of SO$_2$, present at high latitudes and in a polluted plume, are required to allow drawing conclusions.

More generally, the results presented in this work open unexpected perspectives for the monitoring of air quality with TIR satellite sounders, by extending it to other pollutants and other regions with favorable thermal contrast conditions. Recently, a severe pollution episode, that occurred in the North China Plain in January 2013, has been analysed by *Boynard et al.* [2014], who provided simultaneous observations of SO$_2$ and other pollutants by exploiting the enhanced sensitivity of IASI in cases of temperature inversion.

References

386 Allen-Gil, S. M., J. Ford, B. K. Lasorsa, M. Monetti, T. Vlasova, and D. H. Landers (2003),

387   Heavy metal contamination in the Taimyr Peninsula, Siberian Arctic, *The Science of*

388   *the Total Environment*, *301*, 119–138, doi:10.1016/S0048-9697(02)00295-4.

389 AMAP (1998), *Acidifying Pollutants, Arctic Haze, and Acidification in the Arctic*, chap.

390   Chapter 9, pp. 621–659, Arctic Monitoring and Assessment Programme (AMAP).

391 AMAP (2006), *AMAP Assessment 2006: Acidifying Pollutants, Arctic Haze, and Acidi-*

392   *fication in the Arctic*, Arctic Monitoring and Assessment Programme (AMAP).

393 Anderson, G., S. Clough, F. Kneizys, J. Chetwynd, and S. E.P. (1986), AFGL Atmo-

394   spheric Constituent Profiles (0-120km), AFGL-TR-86-0110, *Environmental Research*

395   *Papers*, *954*, ADA175173.

396 August, T., D. Klaes, P. Schlüssel, T. Hultberg, M. Crapeau, A. Arriaga, A. OCarroll,

397   D. Coppens, R. Munro, and X. Calbet (2012), IASI on Metop-A: Operational Level

398   2 retrievals after five years in orbit, *Journal of Quantitative Spectroscopy & Radiative*

399   *Transfer*, *113*, 1340–1371, doi:10.1016/j.jqsrt.2012.02.028.

400 Blacksmith Institutes (2007), The world's worst polluted places - the top ten of the dirty

401   thirty.

402 Blais, J. M., K. E. Duff, T. E. Laing, and J. P. Smol (1999), Regional contamination in

403   lakes from the Noril'sk region in Siberia, Russia, *Water. Air. Soil Pollut.*, *110*, 389–404,

404   doi:10.1023/A:1005059325100.

405 Boyd, R., S.-J. Barnes, P. De Caritat, V. A. Chekushin, V. A. Melezhik, C. Reimann,

406   and M. L. Zientek (2009), Emissions from the coppernickel industry on the

407   Kola Peninsula and at Norilsk, Russia, *Atmos. Environ.*, *43*, 1474–1480, doi:

10.1016/j.atmosenv.2008.12.003.

Boynard, C., A.and Clerbaux, L. Clarisse, S. Safieddine, M. Pommier, M. Van Damme, S. Bauduin, C. Oudot, J. Hadji-Lazaro, D. Hurtmans, and P.-F. Coheur (2014), First space measurements of simultaneous pollutants in the boundary layer from IASI: a case study in the North China Plain, *Geophys. Res. Lett.*, *41*, doi:10.1002/2013GL058333.

Carboni, E., R. Grainger, J. Walker, A. Dudhia, and R. Siddans (2012), A new scheme for sulphur dioxide retrieval from IASI measurements: application to the Eyjafjal-lajökull eruption of April and May 2010, *Atmos. Chem. Phys.*, *12*, 11,861–11,897, doi: 10.5194/acp-12-11417-2012.

Carn, S. A., A. J. Krueger, N. A. Krotkov, and M. A. Gray (2004), Fire at Iraqi sulfur plant emits SO₂ clouds detected by Earth Probe TOMS, *Geophys. Res. Lett.*, *31*(L19105), doi:10.1029/2004GL020719.

Carn, S. A., A. J. Krueger, N. A. Krotkov, K. Yang, and P. F. Levelt (2007), Sulfur dioxide emissions from Peruvian copper smelters detected by the Ozone Monitoring Instrument, *Geophys. Res. Lett.*, *34*(L09801), doi:10.1029/2006GL029020.

Chin, M., and D. J. Jacob (1996), Anthropogenic and natural contributions to tropo-spheric surfate: A global model analysis, *J. Geophys. Res.*, *101*, 18,691–18,699, doi: 10.1029/96JD01222.

Clarisse, L., P.-F. Coheur, A. J. Prata, D. Hurtmans, A. Razavi, T. Phulpin, J. Hadji-Lazaro, and C. Clerbaux (2008), Tracking and quantifying volcanic SO₂ with IASI, the September 2007 eruption at Jebel at Tair, *Atmos. Chem. Phys.*, *8*, 7723–7734, doi:10.5194/acp-8-7723-2008.

Clarisse, L., M. W. Shephard, F. Dentener, D. Hurtmans, K. Cady-Pereira, F. Karagu-

lian, M. Van Damme, C. Clerbaux, and P.-F. Coheur (2010), Satellite monitoring of

ammonia: A case study of the San Joaquin Valley, *J. Geophys. Res.*, *115* (D13302),

doi:10.1029/2009JD013291.

Clarisse, L., Y. R'Honi, P.-F. Coheur, D. Hurtmans, and C. Clerbaux (2011a), Thermal

infrared nadir observations of 24 atmospheric gases, *Geophys. Res. Lett.*, *38* (L10802),

doi:10.1029/2011GL047271.

Clarisse, L., M. Fromm, Y. Ngadi, L. Emmons, C. Clerbaux, D. Hurtmans, and P.-F.

Coheur (2011b), Intercontinental transport of anthropogenic sulfur dioxide and other

pollutants: An infrared remote sensing case study, *Geophys. Res. Lett.*, *38* (L19806),

doi:10.1029/2011GL048976.

Clarisse, L., D. Hurtmans, C. Clerbaux, J. Hadji-Lazaro, Y. Ngadi, and P.-F. Coheur

(2012), Retrieval of sulphur dioxide from the infrared atmospheric sounding interferom-

eter (IASI), *Atmospheric Measurement Techniques*, *5*, 581–594, doi:10.5194/amt-5-581-

2012.

Clerbaux, C., A. Boynard, L. Clarisse, M. George, J. Hadji-Lazaro, H. Herbin, D. Hurt-

mans, M. Pommier, A. Razavi, S. Turquety, C. Wespes, and P.-F. Coheur (2009), Mon-

itoring of atmospheric composition using the thermal infrared IASI/MetOp sounder,

Atmos. Chem. Phys., *9*, 6041–6054, doi:10.5194/acp-9-6041-2009.

Coheur, P.-F., B. Barret, S. Turquety, D. Hurtmans, J. Hadji-Lazaro, and C. Clerbaux

(2005), Retrieval and characterization of ozone vertical profiles from a thermal infrared

nadir sounder, *J. Geophys. Res.*, *110* (D24303), doi:10.1029/2005JD005845.

Council on Ethics for the Government Pension Fund Global (2009), Annual report 2009.

Deeter, M. N., D. P. Edwards, J. C. Gille, and J. R. Drummond (2007), Sensitivity of MOPITT observations to carbon monoxide in the lower troposphere, *J. Geophys. Res.*, *112*(D24306), doi:10.1029/2007JD008929.

Fioletov, V. E., C. A. McLinden, N. Krotkov, M. D. Moran, and K. Yang (2011), Estimation of SO₂ emissions using OMI retrievals, *Geophys. Res. Lett.*, *38*(L21811), doi: 10.1029/2011GL049402.

Fioletov, V. E., C. A. McLinden, N. Krotkov, K. Yang, D. G. Loyola, P. Valks, N. Theys, M. Van Roozendael, C. R. Nowlan, K. Chance, X. Liu, C. Lee, and R. V. Martin (2013), Application of OMI, SCIAMACHY, and GOME-2 satellite SO₂ retrievals for detection of large emission sources, *Journal of Geophysical Research: Atmospheres*, *118*, 11,399–11,418, doi:10.1002/jgrd.50826.

Fukasawa, T., S. Ohta, K. Enomoto, N. Murao, S. Yamagata, T. Shimizu, V. N. Makarov, and I. Rastegaev (2000), Measurement of air pollution in Norilsk, *Polar Meteorology and Glaciology*, *14*, 92–102.

Haywood, J. M., A. Jones, L. Clarisse, A. Bourassa, J. Barnes, P. Telford, N. Bellouin, O. Boucher, P. Agnew, C. Clerbaux, P.-F. Coheur, D. Degenstein, and P. Braesicke (2010), Observations of the eruption of the Sarychev volcano and simulations using the HadGEM2 climate model, *J. Geophys. Res.*, *115*(D21212), doi:10.1029/2010JD014447.

Hilton, F., R. Armante, T. August, C. Barnet, A. Bouchard, C. Camy-Peyret, V. Capelle, L. Clarisse, C. Clerbaux, P.-F. Coheur, A. Collard, C. Crevoisier, G. Dufour, D. Edwards, F. Faijan, N. Fourrié, A. Gambacorta, M. Goldberg, V. Guidard, D. Hurtmans, S. Illingworth, N. Jacquinet-Husson, T. Kerzenmacher, D. Klaes, L. Lavanant, G. Masiello, M. Matricardi, A. McNally, S. Newman, E. Pavelin, S. Payan, E. Péquignot,

S. Peyridieu, T. Phulpin, J. Remedios, P. Schlssel, C. Serio, L. Strow, C. Stubenrauch, J. Taylor, D. Tobin, W. Wolf, and D. Zhou (2012), Hyperspectral Earth observation from IASI - Five Years of Accomplishments, *Bulletin of American Meteorological Society*, *93*, 347–370, doi:10.1175/BAMS-D-11-00027.1.

Hirdman, D., H. Sodemann, S. Eckhardt, J. F. Burkhart, A. Jefferson, T. Mefford, P. K. Quinn, S. Sharma, J. Strm, and A. Stohl (2010), Source identification of short-lived air pollutants in the Arctic using statistical analysis of measurement data and particle dispersion model output, *Atmos. Chem. Phys.*, *10*, 669–693, doi:10.5194/acp-10-669-2010.

Jacob, D. J. (1999), *Introduction to Atmospheric Chemistry*, Princeton University Press.

Karagulian, F., L. Clarisse, C. Clerbaux, A. J. Prata, D. Hurtmans, and P.-F. Coheur (2010), Detection of volcanic SO$_2$, ash, and H$_2$SO$_4$ using the Infrared Atmospheric Sounding Interferometer (IASI), *J. Geophys. Res.*, *115*(D00L02), doi:10.1029/2009JD012786.

Khokhar, M., U. Platt, and T. Wagner (2008), Temporal trends of anthropogenic so$_2$ emitted by non-ferrous metal smelters in Peru and Russia estimated from Satellite observations, *Atmos. Chem. Phys. Disc.*, *8*, 17,393–17,422, doi:10.5194/acpd-8-17393-2008.

Khokhar, M. F., C. Frankenberg, J. Hollwedel, S. Beirle, S. Kühl, M. Grzegorski, W. Wilms-Grabe, U. Platt, and T. Wagner (2004), Satellite remote sensing of atmospheric SO$_2$: Volcanic eruptions and anthropogenic emissions, in *2004 Envisat & ERS Symposium*.

Khokhar, M. F., C. Frankenberg, M. Van Roozendael, S. Beirle, Kühl, A. Richter, U. Platt, and T. Wagner (2005), Satellite observations of atmospheric SO$_2$ from volcanic eruptions during the time-period of 1996-2002, *Advances in Space Research*, *36*, 879–887, doi: 10.1016/j.asr.2005.04.114.

Krotkov, N. A., B. McClure, R. R. Dickerson, S. A. Carn, C. Li, P. K. Bhartia, K. Yang, A. J. Krueger, Z. Li, P. F. Levelt, H. Chen, P. Wang, and D. Lu (2008), Validation of SO$_2$ retrievals from the Ozone Monitoring Instrument over NE China, *J. Geophys. Res.*, *113*(D16S40), doi:10.1029/2007JD008818.

Laj, P., J. Klausen, M. Bilde, C. Plaß-Duelmer, G. Pappalardo, C. Clerbaux, U. Baltensperger, J. Hjorth, D. Simpson, S. Reimann, P.-F. Coheur, A. Richter, M. De Mazière, Y. Rudich, G. McFiggans, K. Torseth, A. Wiedensohler, S. Morin, M. Schulz, J. D. Allan, J. L. Attié, I. Barnes, W. Birmili, J. P. Cammas, J. Dommen, H.-P. Dorn, D. Fowler, S. Fuzzi, M. Glasius, C. Granier, M. Hermann, I. S. A. Isaksen, S. Kinne, I. Koren, F. Madonna, M. Maione, A. Massling, O. Moehler, L. Mona, P. S. Monks, D. Müller, T. Müller, J. Orphal, V.-H. Peuch, F. Stratmann, D. Tanré, G. Tyndall, A. Abo Riziq, M. Van Roozendael, P. Villani, B. Wehner, H. Wex, and A. A. Zardini (2009), Measuring atmospheric composition change, *Atmos. Environ.*, *43*, 5351–5414, doi:10.1016/j.atmosenv.2009.08.020.

Law, K. S., and A. Stohl (2007), Arctic Air Pollution: Origins and Impacts, *Science*, *315*, 1537, doi:10.1126/science.1137695.

Lee, C., R. V. Martin, A. Van Donkelaar, H. Lee, R. R. Dickerson, J. C. Hains, N. Krotkov, A. Richter, K. Vinnikov, and J. J. Schwab (2011), SO$_2$ emissions and lifetimes: Estimates from inverse modeling using in situ and global, space-based (SCIAMACHY and

521 OMI) observations, *J. Geophys. Res.*, *116*(D06304), doi:10.1029/2010JD014758.

522 Li, C., Q. Zhang, N. A. Krotkov, D. G. Streets, K. He, S.-C. Tsay, and J.-F. Gleason

523 (2010), Recent large reduction in sulfur dioxide emissions from Chinese power plants

524 observed by the Ozone Monitoring Instrument, *Geophys. Res. Lett.*, *37*(L08807), doi:

525 10.1029/2010GL042594.

526 Martin, R. V. (2008), Satellite remote sensing of surface air quality, *Atmos. Environ.*, *42*,

527 7823–7843, doi:10.1016/j.atmosenv.2008.07.018.

528 McLinden, C. A., V. Fioletov, K. F. Boersma, N. Krotkov, C. E. Sioris, J. P. Veefkind,

529 and K. Yang (2012), Air quality over the Canadian oil sands: A first assessment using

530 satellite observations, *Geophys. Res. Lett.*, *39*(L04804), doi:10.1029/2011GL050273.

531 Rodgers, C. D. (2000), *Inverse Methods for Atmospheric Sounding: Theory and Practice*,

532 World scientific.

533 Rothman, L., I. Gordon, A. Barbe, D. ChrisBenner, P. Bernath, M. Birk, V. Boudon,

534 L. Brown, A. Campargue, J.-P. Champion, K. Chance, L. Coudert, V. Dana, V. Devi,

535 S. Fally, J.-M. Flaud, R. Gamache, A. Goldman, D. Jacquemart, I. Kleiner, N. Lacome,

536 W. Lafferty, J.-Y. Mandin, S. Massie, S. Mikhailenko, C. Miller, N. Moazzen-Ahmadi,

537 O. Naumenko, A. Nikitin, J. Orphal, V. Perevalov, A. Perrin, A. Predoi-Cross, C. Rins-

538 land, M. Rotger, M. Šimečková, M. Smith, K. Sung, S. Tashkun, J. Tennyson, R. Toth,

539 A. Vandaele, and J. VanderAuwera (2009), The *HITRAN* 2008 molecular spectroscopic

540 database, *Journal of Quantitative Spectroscopy & Radiative Transfer*, *110*, 533–572,

541 doi:10.1016/j.jqsrt.2009.02.013.

542 Schlüssel, P., T. H. Hultberg, P. L. Phillips, T. August, and X. Calbet (2005), The

543 operational IASI Level 2 processor, *Advances in Space Research*, *36*, 982–988, doi:

544   10.1016/j.asr.2005.03.008.

545 Tutubalina, O., and W. Rees (2001), Vegetation degradation in a permafrost region as

546   seen from space: Norilsk (19611999), *Cold Regions Science and Technology*, *32*, 191–203,

547   doi:10.1016/S0165-232X(01)00049-0.

548 Van Damme, M., L. Clarisse, C. L. Heald, D. Hurtmans, Y. Ngadi, C. Clerbaux, A. J.

549   Dolman, J. W. Erisman, and P.-F. Coheur (2013), Global distributions and trends

550   of atmospheric ammonia (NH₃) from IASI satellite observations, *Atmos. Chem. Phys.*

551   *Disc.*, *13*, 24,301–24,342, doi:10.5194/acpd-13-24301-2013.

552 Vlasova, T. M., B. I. Kovalev, and Philipchuk (1991), Effects of point source atmospheric

553   pollution on boreal forest vegetation of Northern Siberia, in *Proceedings of the Inter-*

554   *national Conference on the Role of the Polar Regions in Global Change*, vol. 2, pp.

555   423–428.

556 Walter, D., K.-P. Heue, A. Rauthe-Schöch, C. A. M. Brenninkmeijer, L. N. Lamsal,

557   N. A. Krotkov, and U. Platt (2012), Flux calculation using CARIBIC DOAS air-

558   craft measurements: SO₂ emission of Norilsk, *J. Geophys. Res.*, *117*(D11305), doi:

559   10.1029/2011JD017335.

560 Wesely, M. L. (2007), Parameterization of surface resistances to gaseous dry de-

561   position in regional-scale numerical models, *Atmos. Environ.*, *41*, S52–S63, doi:

562   10.1016/j.atmosenv.2007.10.058.

563 Zubareva, O. N., L. N. Skripalshchikova, N. V. Greshilova, and V. I. Kharuk

564   (2003), Zoning of Landscapes Exposed to Technogenic Emissions from the Norilsk

565   Mining and Smelting Works, *Russian Journal of Ecology*, *34*(6), 375–380, doi:

566   10.1023/A:1027356316112.
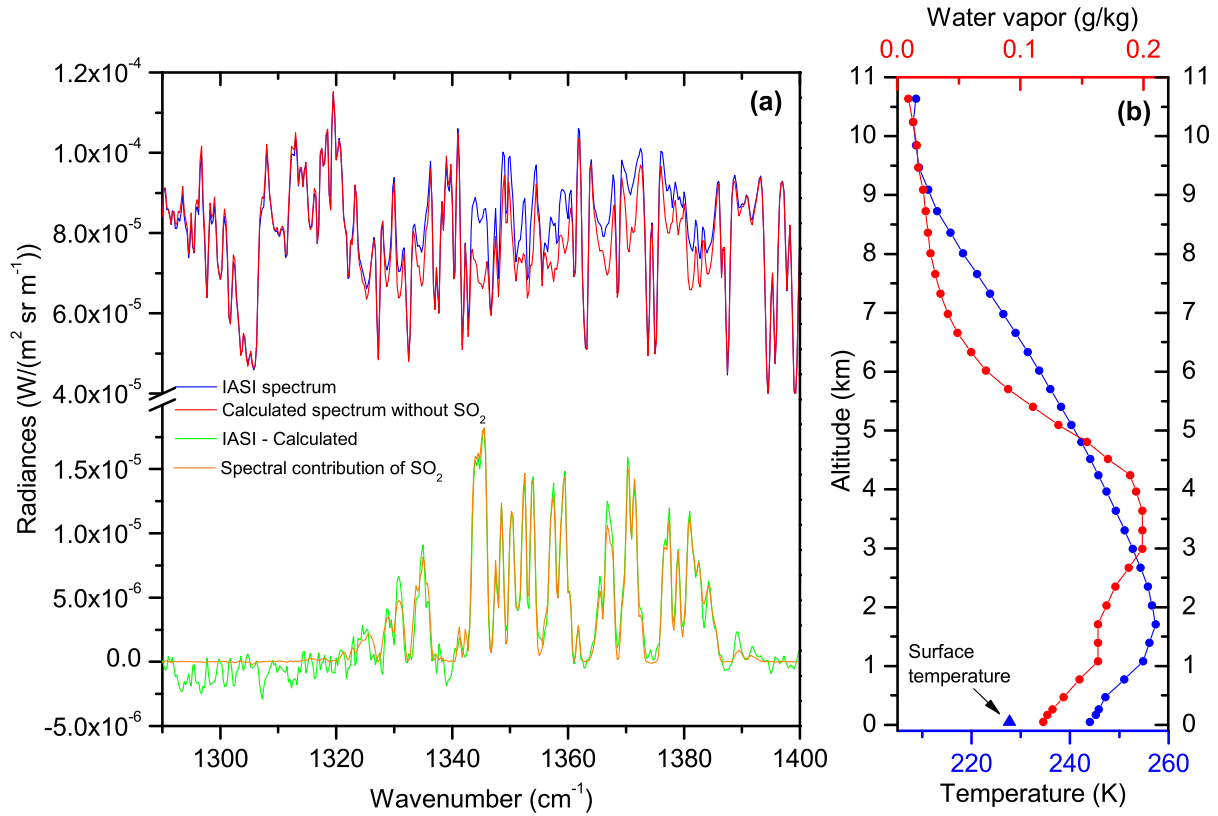
Figure 1. (a) IASI spectrum (W/(m^2 sr m^{-1})) recorded on the 9th of February 2010 in the area of Norilsk (blue). Water vapor and CH$_4$ profiles have been retrieved from it and then used in the simulation of a corresponding spectrum for an atmosphere containing no SO$_2$ (red). The residual of the two is the green curve and shows only SO$_2$ spectral features in emission. The spectral contribution of SO$_2$ to the spectrum is shown in orange. (b) Associated temperature (K, blue), water vapor (g/kg, red) profiles and ground temperature (K, blue triangle) provided by the Eumetsat's Data Distribution System (EumetCast). These data have been used to simulate the IASI spectrum (red) in (a). The thermal contrast (defined as the difference between the surface temperature and the first available atmospheric temperature) for this particular case is -16.3 K.
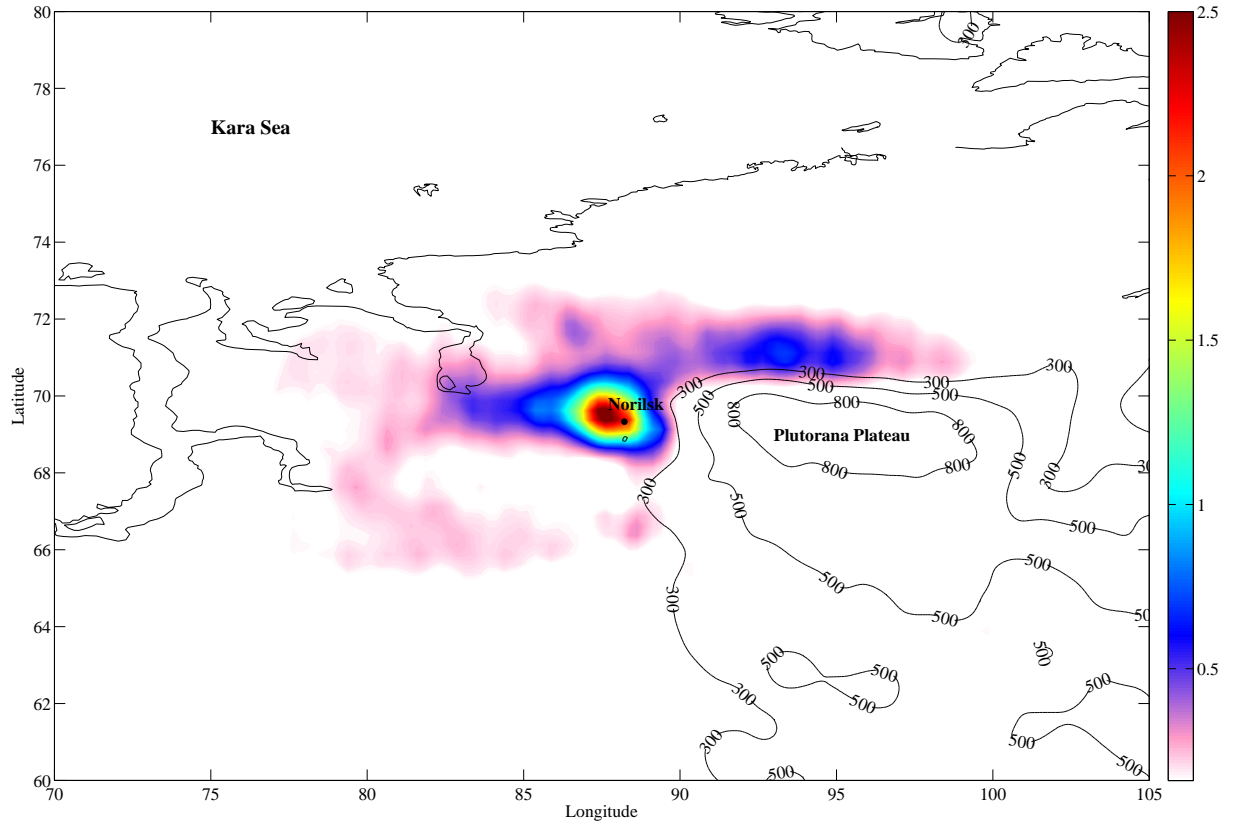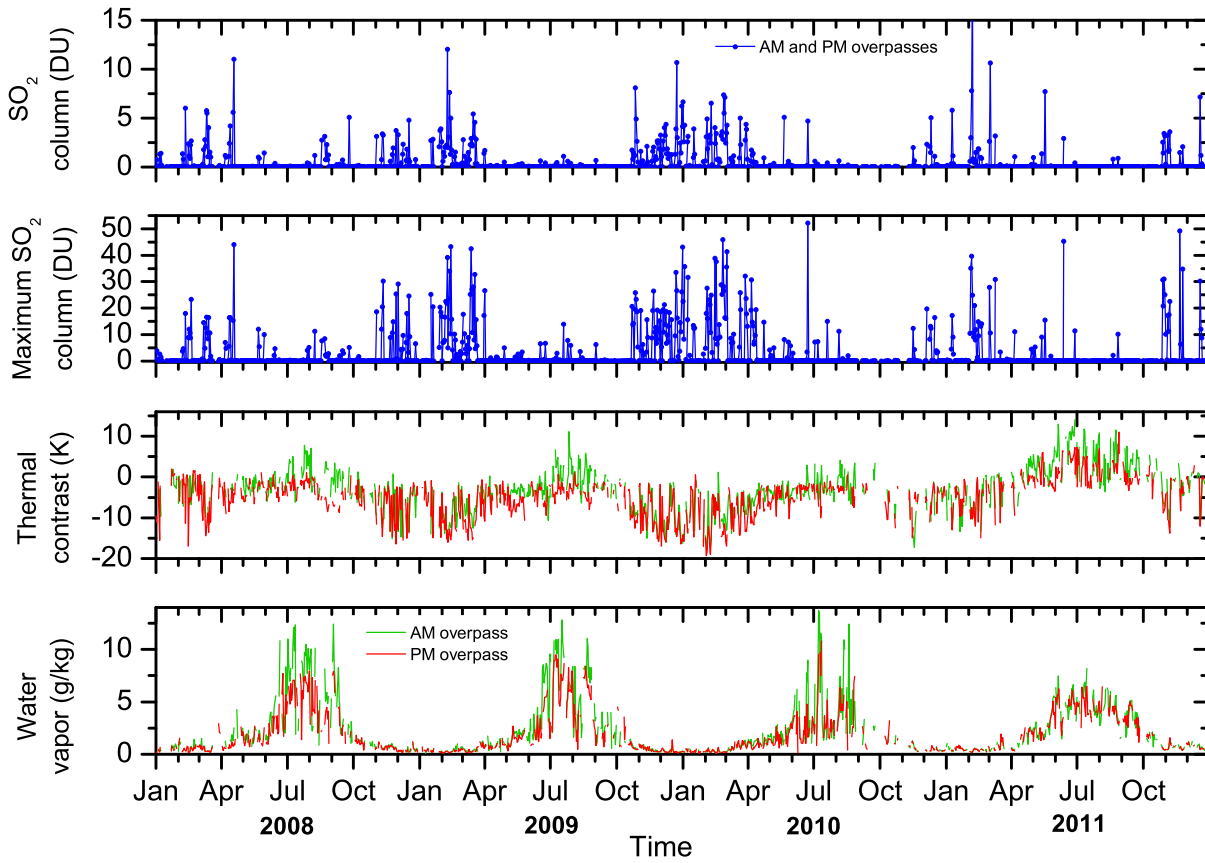
Figure 2. Distribution of the average retrieved 0–2 km SO$_2$ columns over the Norilsk region for February 2009, expressed in Dobson Units. The average have been performed on a $0.25° \times 0.25°$ grid and then interpolated. The contour on the plot shows the terrain height in meters.

Figure 3. From top to bottom: daily average retrieved SO$_2$ columns (0–2 km), expressed in DU; daily maximum SO$_2$ columns (0-2 km, DU); daily average thermal contrasts, calculated as the difference between the surface temperature and the temperature at 350 m above the ground; daily average water vapor amount at 350 m, expressed in g/kg. All averages have been calculated for data in a circle of 50 km radius centered on Norilsk, for the period 01/01/2008–31/12/2011. Data from morning and evening IASI overpasses have been simultaneously averaged for SO$_2$ columns and the distinction is made for the thermal contrast and water vapor. Note that some measurements are missing for some days. They correspond to gaps in the data or cloudy scenes and have therefore been filtered.

Table 1. Comparison between different available SO$_2$ measurements made in the Norilsk region. The slant column density correspond to the SO$_2$ concentration integrated along the light path. SO$_2$ volume mixing ratios (vmrs) and concentrations given for this work have been calculated from the IASI retrieved 0-2 km columns. They respectively represent the mean vmr and the mean concentration of SO$_2$ in the 0-2 km atmospheric layer.

	SO$_2$ measurements	Period	Comments
This work	Daily winter averages of the 0–2 km column, of the 50 km radius area around Norilsk, fluctuate:	2008–2011	Satellite (IASI)
	10–30 ppb, maximum of 105 ppb		
	20–75 μg/m^3, maximum of 280 μg/m^3		
	0.4–1.5 $\times$ 10^{17} molecules/cm^2, maximum of 5 $\times$ 10^{17} molecules/cm^2		
Fukasawa et al. [2000]	Half month averages fluctuating between 30 and 60 ppb	April-December 1995	Surface
	Maximum averages of 140 ppb		
Khokhar et al. [2004, 2005]	Slant column density of about 2 $\times$ 10^{16} molecules/cm^2	Average over 1996–2002	Satellite (GOME)
AMAP [2006]	Annual averages fluctuate between 70 and 210 μg/m^3	1990–2003	
Walter et al. [2012]	Slant column density of about 8 $\times$ 10^{17} molecules/cm^2 at about 5km of Norilsk	22th October 2010	Aircraft
	Vertical column density in the range of 0.5–2 $\times$ 10^{17} molecules/cm^2		Satellite (OMI)
Fioletov et al. [2013]	Average values of 5.4–6.7 $\times$ 10^{16} molecules/cm^2	2005–2010 (depends on instrument)	Satellite (OMI, SCIAMACHY, GOME-2)

Table 2.   Norilsk's winter emissions derived from IASI SO$_2$ measurements. Emissions obtained in other studies are also presented. For all, the period and the chosen lifetime (if required in the study) are given. Winter includes 5 cold months: January, February, March, November and December.

	Period	Lifetime	Emissions	Comments
			Winter/yearly	
This work	2009	3 days	0.46 Mt/1.10 Mt	Satellite (IASI)
Fioletov et al. [2013]	2005–2007	5 hours	2.65±0.61 Mt per year	Satellite (OMI, SCIA-MACHY, GOME-2)
	2008–2010	5 hours	2.27±0.96 Mt per year	
Walter et al. [2012]	2010	-	0.92 Mt per year (0.41–1.46 Mt depending on chosen parameters)	Aircraft (CARIBIC)
	2010	1 day	0.7 Mt per year (0.6–0.9 Mt depending on the area of calculation)	Satellite (OMI)
Khokhar et al. [2008]	1996–2002	1 day	1.685±0.3 Mt per year	Satellite (GOME)
Blacksmith Institutes [2007]	-	-	2 Mt per year	
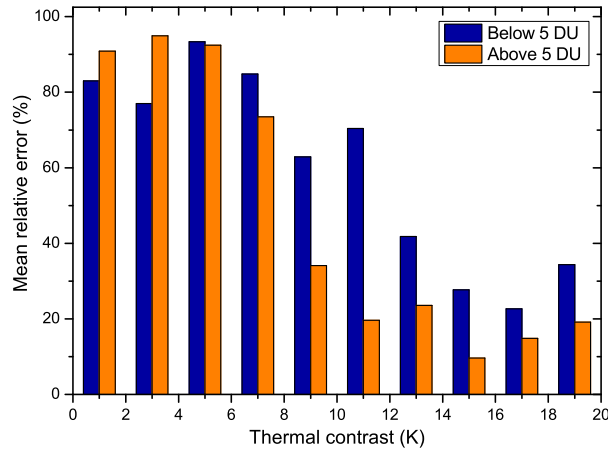
Figure 4. Histogram of the relative error on the 0–2 km SO$_2$ column as a function of thermal contrast (absolute value). The relative error is calculated according to the relation: $[(SO_2\ column)_{true} - (SO_2\ column)_{retrieved}]/(SO_2\ column)_{true} \times 100\%$. Bars represent the mean error calculated for fields of 2 K range of thermal contrast. The blue bars are the mean error for columns smaller than 5 DU and the orange are the mean error for columns larger than 5 DU.